Pergamon

Int. J. Heat Mass Transfer. Vol. 41, Nos 6–7, pp. 859–869, 1998

Printed in Great Britain
0017–9310/98 $19.00 + 0.00

PII: S0017–9310(97)00178–6

Modeling of heat conduction within chamber walls for multidimensional internal combustion engine simulations

YONG LIU and R. D. REITZ†

Engine Research Centre, University of Wisconsin, Madison, 1500 Engineering Drive, Madison, WI 53705, U.S.A.

(*Received* 21 *November* 1996 *and in final form* 7 *June* 1997)

Abstract—A two-dimensional (axisymmetric) transient heat conduction in components computer program (HCC) was successfully developed for predicting engine combustion chamber wall temperatures. The alternating direction explicit (ADE) Saul'yev method, an explicit, unconditionally stable finite difference method, was used in the code. Special treatments for the head gasket and the piston-liner air gap, the piston movement, and a grid transformation for describing the realistic piston bowl shape were designed and utilized. The results were compared with a finite element method and were verified to be accurate for simplified test problems. In addition, the method was applied to realistic problems of heat transfer in an Isuzu engine and a Caterpillar diesel engine, and gave good agreement with available experimental measurements. © 1997 Elsevier Science Ltd.

INTRODUCTION

It is known that heat transfer effects internal combustion engine performance, efficiency, and emissions. As far as performance is concerned, cooling for the cylinder head, cylinder, and piston is desired because of problems such as thermal stresses in regions of high heat flux, deterioration of the lubricating oil film, and knock and preignition in spark ignition engines. On the other hand, an increase of heat transfer to the combustion chamber walls will lower the gas temperature and pressure within the cylinder, and this reduces the work per cycle transferred to the piston. Heat transfer from the working gas to the cooling system of a conventional diesel engine accounts for up to 30% of the fuel energy. About 50% of this energy is lost through the piston and 30% through the head [1]. Thus efficiency is affected by the magnitude of engine heat transfer. Changes in gas temperature due to the heat transfer also impact pollutant emission formation processes. Generally, a higher temperature in the cylinder during combustion can cause an increment in NO_x emissions, but a lower temperature may promote the formation of particulates, or soot. Therefore, in the sense of emission control, more attention should be paid to engine heat transfer.

Since heat transfer is so important in engines, almost all the computer programs for multidimensional simulation of combustion in engines contain heat transfer models. The KIVA-II code [2] describes chemically reactive flow with sprays and is extensively used in engine combustion simulations. It has the ability to calculate the flows in engine cylinders with arbitrarily shaped piston geometries, including the effects of turbulence and wall heat transfer. In heat transfer models of the KIVA-II code, the chamber wall temperature T_w is a vital parameter for determining magnitude of heat flux. If an accurate wall temperature distribution is unavailable, even with an improved temperature wall function [3], it is still impossible to obtain accurate heat flux results. In general, the combustion chamber of an internal combustion engine is formed by the cylinder wall, head, and piston, and the temperature distributions are different for each surface. Typically, the temperature of each surface is assumed to be a constant [2]. This is not consistent with the actual situation occurring on the surfaces of the combustion chamber.

In order to obtain the temperature distribution on the chamber surfaces, a method was developed in this work to calculate the temperature distribution using the heat conduction equations. With the component material property data and appropriate boundary conditions a temperature distribution, instead of an assumed wall temperature, is obtained which is used in the KIVA multidimensional combustion code. This approach allows more accurate simulations of engine combustion and heat transfer.

MODELS AND NUMERICAL METHODS

The approach to determine the combustion chamber temperature distributions is deduced from the energy conservation law. For simplicity it is assumed that the engine geometry is axisymmetric. In two-

† Author to whom correspondence should be addressed.

NOMENCLATURE

b	distance between piston top surface and piston pin axis
c_p	heat capacity
h	finite difference parameter
k	conductivity
l	connecting rod length, finite difference parameter
N	rotational speed
q''	heat flux
r	radial coordinate, crank radius
s	piston position, arc length along piston surface
s_c	squish height
t	time
T	temperature
U	temperature computed from left to right/bottom to top
v_p	piston velocity
V	temperature computed from right to left/top to bottom
z	axial coordinate.

Greek symbols

α	thermal diffusivity of wall material, $k/\rho c_p$
η, ξ	coordinate mapping functions
θ	crank angle.

Subscripts

w	wall
p	piston.

dimensional cylindrical coordinates the heat conduction equation is

$$\frac{1}{r}\frac{\partial}{\partial r}\left(kr\frac{\partial T}{\partial r}\right)+\frac{\partial}{\partial z}\left(k\frac{\partial T}{\partial z}\right)=\rho c_p\frac{\partial T}{\partial t} \quad (1)$$

where r and z are the coordinates in the radial and axial directions, respectively; T is the wall temperature; k is the thermal conductivity; ρ is the material density; c_p is the specific heat; and t is time.

As the boundary conditions, the temperatures on the outer surfaces of the cylinder wall liner, head and piston were treated as constant surface temperature conditions, in which the temperature equals either the measured coolant temperature or the oil temperature in the crankshaft case. This is reasonable because the variation of the temperature on these surfaces is much smaller than that on the inner surfaces of the combustion chamber. The boundary condition on the inner gas-side surface of the combustion chamber was a specified heat flux, which was obtained through experiments or through KIVA-II predictions.

The numerical method used is the alternating direction explicit (ADE) Saul'yev finite difference method [4]. This method is characterized by being explicit, unconditionally numerically stable, and accurate. For the constant coefficient heat conduction equation, $T_t = \alpha T_{xx}$, where $\alpha = k/\rho c_p$ is the thermal diffusivity, the Saul'yev finite difference expression is [5]

$$\frac{U_j^{n+1}-U_j^n}{\Delta t}=\alpha\frac{\partial}{\partial x}\left(\frac{\partial U}{\partial x}\right)=\frac{\alpha}{\Delta x}\left(\frac{\partial U}{\partial x}\bigg|_{j+1/2}^{n}-\frac{\partial U}{\partial x}\bigg|_{j-1/2}^{n+1}\right)$$

where j is a discretized spatial coordinate, n is the temporal coordinate and $U_j^n = T_j^n$. With $d = \alpha\Delta t/\Delta x^2$ (i.e. uniform mesh spacing Δx)

$$U_j^{n+1} = U_j^n + d(U_{j+1}^n - U_j^n - U_j^{n+1} + U_{j-1}^{n+1}). \quad (2)$$

Provided that the calculation sweeps in the direction of increasing j, U_j^n, U_{j+1}^n and the advance time value U_{j-1}^{n+1} are already known, and eqn (2) can be conveniently used to calculate U_j^{n+1}. Although it is a two-level method, it requires only one storage array, since the same memory location can be used for U_j^{n+1} and U_j^n in the replacement statement [eqn (2)]. Since eqn (2) can be solved for U_j^{n+1}, the method is explicit.

To control the truncation error, the direction of the calculation sweep is also reversed in the direction decreasing j, giving a formula for $V_j^n = T_j^n$

$$V_j^{n+1} = V_j^n + d(V_{j+1}^{n+1} - V_j^{n+1} - V_j^n + V_{j-1}^n)$$

and, finally, the advanced time level solution is given by

$$T_j^{n+1} = \tfrac{1}{2}(U_j^{n+1} + V_j^{i+1}). \quad (3)$$

The unconditional stability of the Saul'yev method can be readily proved using the von Neumann method based on Fourier analysis [5].

The method is readily extended to the two-dimensional case with a non-uniform grid arrangement in the r, z and t directions.

Let

$$h_1 = r_i - r_{i-1} = \Delta r_{i-1}; h_2 = r_{i+1} - r_i = \Delta r_i;$$
$$h = h_1 + h_2 = \Delta r_i + \Delta r_{i-1}; \quad l_1 = z_j - z_{j-1} = \Delta z_{j-1};$$
$$l_2 = z_{j+1} - z_j = \Delta z_j; l = l_1 + l_2 = \Delta z_{j-1} + \Delta z_j.$$

then from eqn (1)

$$\frac{U_{i,j}^{k+1}-U_{i,j}^{k}}{\Delta t}$$

$$\approx \frac{2\alpha}{h_1 h_2 h}\left[h_1\left(1+\frac{h_2}{2r_i}\right)(U_{i+1,j}^{k}-U_{i,j}^{k})\right.$$

$$\left.-h_2\left(1-\frac{h_1}{2r_i}\right)(U_{i,j}^{k+1}-U_{i-1,j}^{k+1})\right]$$

$$+\frac{2\alpha}{l_1 l_2 l}[l_1(U_{i,j+1}^{k}-U_{i,j}^{k})-l_2(U_{i,j}^{k+1}-U_{i,j-1}^{k+1})] \quad (4)$$

and a similar equation is written for the opposite sweep direction for use in eqn (3).

In practical engines there are gaps between the cylinder wall, head and piston. The gap between cylinder and head is filled with gasket material and the gap between the cylinder wall (liner) and piston is occupied by piston rings and crevice gas, alternately. In order to form a global finite difference code for the cylinder wall, head and piston, one of the key problems is to develop a method that is able to handle those very thin gaps reasonably and correctly. The distance between cylinder wall and head is usually less than 1 mm for a middle sized engine and that between the cylinder wall and piston is less than 0.5 mm for smaller engines [7]. Since the gas temperature within the cylinder can reach thousands of degrees, it is expected that the temperature gradient within the gaps could be very large. Since an accurate prediction of the temperature distribution is desired, fine grids should be formed within the gaps and this requires non-uniform grids and an absolutely stable difference method is preferable.

The minimum grid dimension in regions of increased spatial resolution was about 0.1 mm in this study. In the region between the cylinder wall and head, a constant conductivity representative of the gasket material is used. In the region between the cylinder wall (liner) and piston, however, air conductivity is used in cases where crevice gas exists, and the conductivity of carbon steel is used to represent the piston rings when the piston is located over that portion of the liner.

Piston movement is a complicating feature that characterizes engine operation and is important in the heat conduction problem. Assume that the connecting rod length is l, crank radius is r, crank angle is θ, then according to Fig. 1(a) [7]

$$s = r(1-\cos\theta)+l-(l^2-r^2\sin^2\theta)^{1/2} \quad (5)$$

$$z_p = r\cos\theta+(l^2-r^2\sin^2\theta)^{1/2}+b \quad (6)$$

$$v_p = 2\pi rN\sin\theta\left[1+\frac{r\cos\theta}{(l^2-r^2\sin^2\theta)^{1/2}}\right] \quad (7)$$

where s_c is the squish height; s is the piston position; z_p is the distance between the crank axis and the piston top surface; v_p is the instantaneous piston velocity; N is the rotational speed of the crankshaft; and b is the distance between the piston top surface and the piston pin axis.

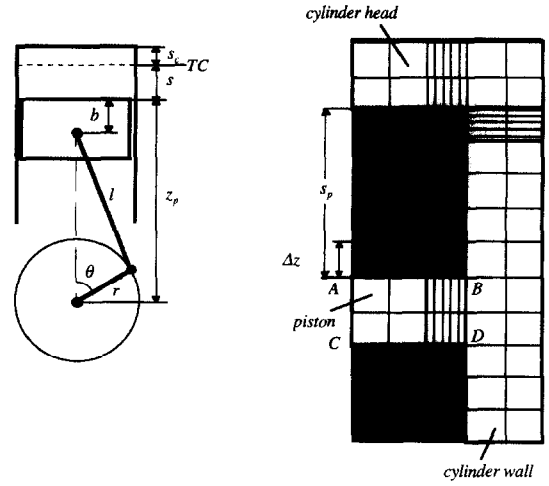

Fig. 1. Schematic diagrams showing (a) geometrical relationships of piston movement; (b) grid distribution in an engine cylinder.

In this study a special technique was developed to solve the moving boundary problem of engine pistons. Firstly, grids were formed in a cylindrically symmetric domain where the left side represents the center line of the engine cylinder. Nodes representing boundaries or inner points of the cylinder wall, head and piston were determined. These nodes participate in the computation and are termed computed nodes, but others outside the boundaries are non-computed nodes. In Fig. 1(b) the nodes in the white regions are the computed nodes and the nodes in shadowed regions are the non-computed nodes. This figure also shows schematically the fine grids (exaggerated) used in the gaps between the cylinder wall, head and piston, discussed in the previous section.

The computed nodes representing the piston and the gap between the piston and cylinder wall [region ABCD in Fig. 1(b)] are separated from other computed nodes. When the engine is running, the piston position s is determined using eqn (5). If $s+s_c$ is moved to $s_p-\Delta z$ in the next time step [see Fig. 1(b)], the nodes just above the piston top boundary AB are converted (i.e. snapped [2]) into the nodes of a new top boundary and the nodes on the former bottom boundary CD are changed into non-computed nodes. Meanwhile, temperatures at each node at the former piston position are moved to the corresponding node at the new piston position. In this way the upward piston movement is realized in the finite difference analysis. Downward piston movement is treated with an analogous method.

Instead of a flat-topped piston such as that typically used in spark-ignition engines, diesel engines usually have a piston with bowl. In medium-to-small size

direct-injection diesel engines, use of a bowl-in-piston combustion chamber results in substantial swirl amplification at the end of the compression process. The effect of air swirl on the performance and emissions characteristic of this type of engine is very important.

In order to describe the configuration of a bowl-shaped piston in the finite difference representation, tabular information about the piston outline is used [i.e. the coordinates r_i and z_i in Fig. 2(a)]. In the present study the bowl axis is assumed to be concentric with the axis of the cylinder. The piston configuration used is a simplified one, as shown in Fig. 2(b), where the white portion is the piston body with conductivity the same as the piston metal material and the shadowed portions are piston air cavities with air conductivity.

The finite difference equations are most efficiently solved in a rectangular domain. Thus, it is convenient to transform the nonrectangular physical domain to a rectangular computational domain. Figure 2(c) shows the physical domain in the r and z coordinate system and also the computational domain of the piston in the η and ξ coordinate system. From the geometry characteristics, the relationship between the physical and the computational domain can be defined as

$$\xi = \xi(r, z) = r \tag{8}$$

$$\eta = \eta(r, z) = z - \left[\frac{z_{i+1} - z_i}{r_{i+1} - r_i}(r - r_i) + z_i\right] \qquad (r_i < r < r_{i+1}) \tag{9}$$

where $\xi = \xi(r, z)$, and $\eta = \eta(r, z)$ are mapping functions.

The transformed finite difference equations for use in eqn (3) are given in Appendix A. In addition to the transformation for the inner nodes on the piston, it is also necessary to transform the boundary conditions from the physical to the computational domains. The possible boundary node configurations are shown in Fig. 3, and the appropriate boundary finite difference equations are given in Appendix B.

It was mentioned previously that it is necessary to refine the finite difference grid to simulate the gap between the piston and cylinder wall, as well as the gasket between the cylinder wall and head. Morel *et al.* [8] studied cyclical thermal phenomena near engine combustion chamber surfaces, and concluded that the heat flux from the gases to the wall of engines is highly transient, producing temperature transients in thin layers of the wall adjacent to the combustion chamber. In order to include these characteristics of temperature transience into the present computational code, the grid adjacent to the inner surfaces of the cylinder wall, head and piston must also be refined.

Figure 4(a) shows an example where the grid adjacent to the gas-side of the cylinder wall, head and piston is refined. For the cylinder wall and head, it is relatively simple; it is only necessary to increase the

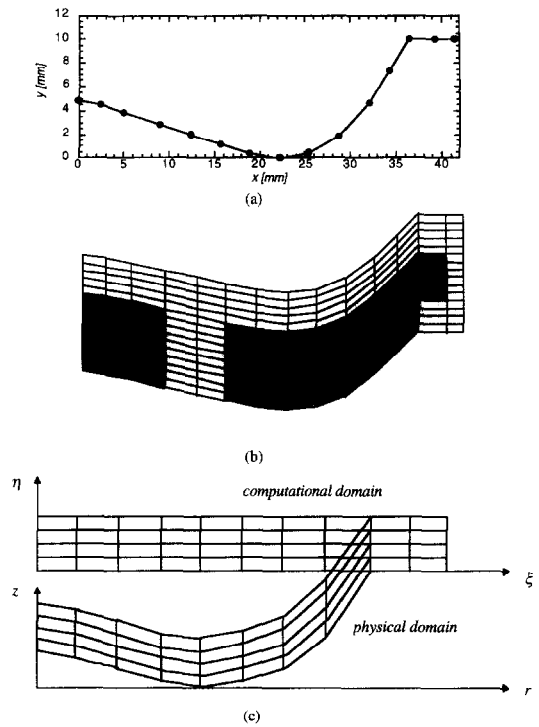

Fig. 2. (a) Silhouette of piston bowl; (b) piston grid layout; (c) physical and computational domains of the piston grid.

grid density in the region near the inner surface. For the piston, however, the circumstances are much more complicated and difficult. Simply increasing the grid density adjacent to the surface of the piston [as shown by the dash-lines in Fig. 4(a)] causes the grids in the piston not to match the grids in the cylinder wall, which complicates the finite difference computation. Increasing the grid density in the cylinder wall to make

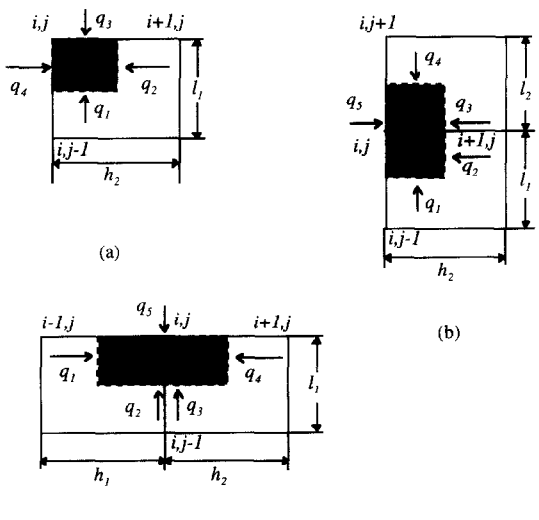

Fig. 3. Boundary nodes used in the grid transformation.

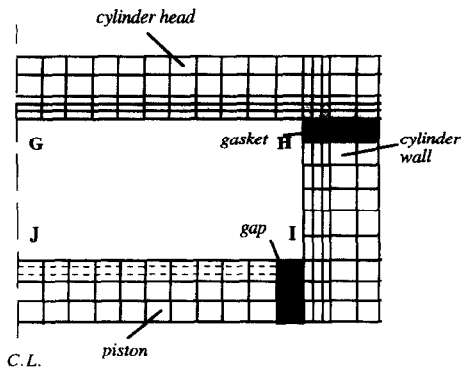

(a)

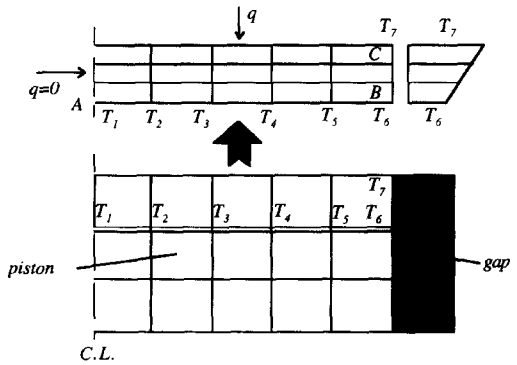

(b)

Fig. 4. (a) Fine grid specification in the cylinder wall and head; (b) fine grid specification in the piston.

them match the fine grids in the piston, causes them not to match the regular grids in the piston. To overcome this difficulty, a kind of separation method was employed, as shown in Fig. 4(b). As the first step the finite difference equation is solved with the regular coarse grid, and the temperature distribution along the double solid line (AB) shown in Fig. 4(b) is obtained. Then in a second step part of the piston along the double solid line is cut off and analyzed as a separate individual computational region with its own boundary conditions: adiabatic along the cylinder axis, the known temperature along boundary AB, and a linear temperature distribution along boundary BC and known heat flux from the gas-side in the combustion chamber. This method of grid refinement gives a more accurate estimation of the surface temperature of the piston.

The width (thickness) of the region of the denser surface grid was chosen (based on estimates of the thermal boundary layers in the metal components) to be larger than the thermal boundary layer thickness. A procedure was also developed whereby a coarse grid was used for computational efficiency for engine cycles early in the transient engine warm-up process. When a pseudo-steady state was reached, the fine grid blocks were introduced to resolve the detailed cyclic transient heat transfer processes in the gas-side wall regions.

RESULTS AND DISCUSSION

In order to validate the present heat conduction in components (HCC) code, various simplified test problems were analyzed, including one- and two-dimensional problems [9]. For example, Fig. 5 shows heat conduction predictions in a one-dimensional slab (conductivity $k = 53.1$ W m^{-1} K^{-1}, density $\rho = 7870$ kg m^{-3} and specific heat $c_p = 447$ J kg^{-1} K^{-1}) which

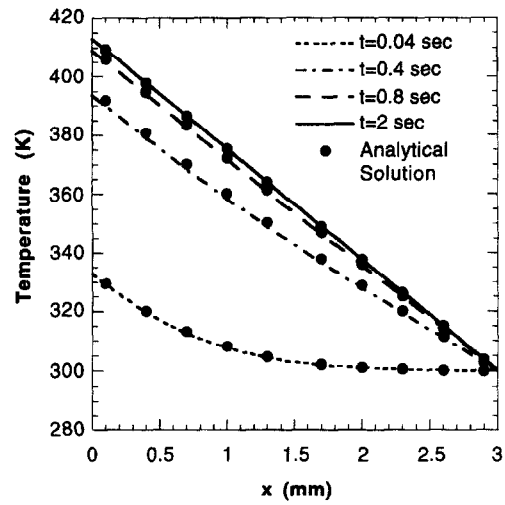

(a)

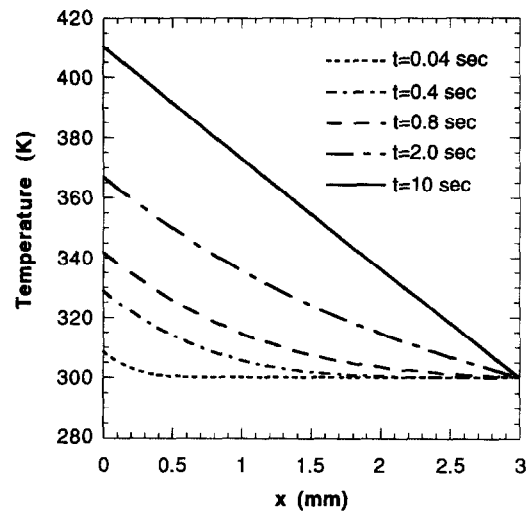

(b)

Fig. 5. Computed result of one-dimensional heat conduction in a slab using the present HCC code with various numerical timesteps (a) $\alpha\Delta t/\Delta x^2 = 0.1$; (b) $\alpha\Delta t/\Delta x^2 = 10$.

is 3 mm thick. The slab is initially at uniform temperature equal to that on the right-side boundary ($T_r = 300$ K) and a steady heat flux ($q'' = 2$ MW m^{-2}) instantaneously enters the wall from the left side at time $t = 0$. Figure 5(a) shows that the temperature within the wall changes from uniform to a linear distribution. By $t = 2$ s, the temperature of the left boundary is predicted to be 413 K, which is the same as the analytical steady solution ($T_l = 413$ K, calculated from the Fourier equation $q'' = k/l(T_l - T_r)$) and also the same as the result of finite element method computation FEHT [10]. For the computed results in Fig. 5(a) the grid spacing was $\Delta x = 0.1$ mm, and the numerical timestep used was $\Delta t = 6.625 \times 10^{-5}$ (i.e. $\alpha\Delta t/\Delta x^2 = 0.1$). The analytical solutions of this problem [11] are also shown in Fig. 5(a) and are seen to be very consistent with the numerical solutions.

Other computations were also made with much larger numerical timesteps (e.g. $\alpha\Delta t/\Delta x^2 = 10$), which give similar steady state results, shown in Fig. 5(b). The results verify that the Saul'yev method gives the correct steady state solution even when $\alpha\Delta t/\Delta x^2 \gg 1/2$, and the method has good stability characteristics. For the transient processes, the temperature distributions are somewhat different for large $\alpha\Delta t/\Delta x^2$ values, which indicates an influence of Δt on transient accuracy.

Two-dimensional test problems have also been considered [9] such as heat conduction in the configuration of the cylinder wall, head and piston of an I.C. engine, as shown in Fig. 4(a). In this case the piston was stationary and the material was an aluminum alloy with conductivity $k = 185$ W m^{-1} K^{-1}, density $\rho = 2790$ kg m^{-3} and specific heat $c_p = 883$ J kg^{-1} K^{-1}; the temperature on the outer boundaries was 353 K and the symmetry axis was adiabatic. The surface heat flux along GHIJ [see Fig. 4(a)] was given to be 3 MW m^{-2} and the timestep used was $\Delta t = 1.0 \times 10^{-6}$ s (i.e. $\alpha(\Delta t/\Delta r^2 + \Delta t/\Delta z^2) = 1.135 \times 10^{-3}$.

Figure 6 shows a comparison between the chamber surface temperatures computed by the present HCC finite difference method (120 nodes) and that by the finite element method (using FEHT [10], with 120 nodes). In this figure the s coordinate is an extended broken line, which represents the location along the chamber surface from point G to J through H and I, as shown in Fig. 4(a). The results obtained by the two different methods match each other very well. The test problem results give confidence to the use of the present HCC code for engine wall temperature predictions.

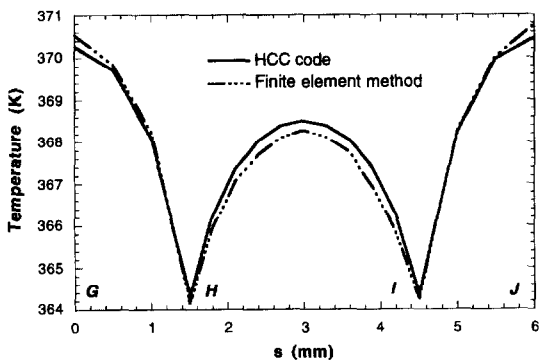

Fig. 6. Computed combustion chamber wall surface temperature distribution in the engine model test problem [see Fig. 4(a)]: (a) using the present HCC code; (b) comparison between HCC and finite element method.

The maximum temperature appears on the cylinder head and the piston, and the location is near the center line (symmetry axis) of the cylinder, as expected. In the mid-point of the cylinder wall there also exists a high temperature. Note that in the corners the temperature is a little lower than at other positions. This indicates that under the condition of uniform heat flux, the corners of the cross-section of an engine cylinder have a higher heat transfer effect.

One of the engines studied was an Isuzu diesel engine developed by Isuzu Ceramics Research Institute (ICRI). It is a ceramic, single cylinder DI diesel engine. The main engine specifications are given in Table 1. The piston crown, head, liner, cylinder and valves are made of Silicon Nitride (Kyocera SN235). This material has the following properties at room temperature: density $\rho = 3240$ kg m^{-1}; thermal conductivity $k = 31$ W m^{-1} K^{-1}; and specific heat $c_p = 680$ J kg^{-1} K^{-1}. Additional insulation is provided by air gaps and insulating rings between the ceramics and the metal components of the engine. The intake and exhaust ports are also insulated. The engine has limited cooling of the cylinder wall and of the bottom of the metal skirt of the piston. Both of these regions are cooled by the lubricating oil.

According to the above specifications and known operating conditions [12], a simplified finite difference model of this engine was set up. Figure 7(a) shows the grids and boundary conditions of the model for the fine grid option (the coarse grid option has no fine grids near the combustion chamber inner surfaces). The grid number in the r-direction is 34 for the fine grid option, which includes four grids within the piston-liner air gap. The grid size in the r-direction depends on the piston silhouette and the distribution of its outline points (it is 0.1 mm within the air gap, and 0.05, 0.1 or 1 mm with increasing depth below the cylinder wall). The grid number in the z-direction, however, is much more than that in the r-direction

Table 1. Specifications of Isuzu ceramic diesel engine

Bore of cylinder	84	mm
Stroke	92	mm
Squish	1.3	mm
Compression ratio	12.6	
Connecting rod length	193	mm
Piston crown	shallow dish	—
Engine speed	1500	rpm

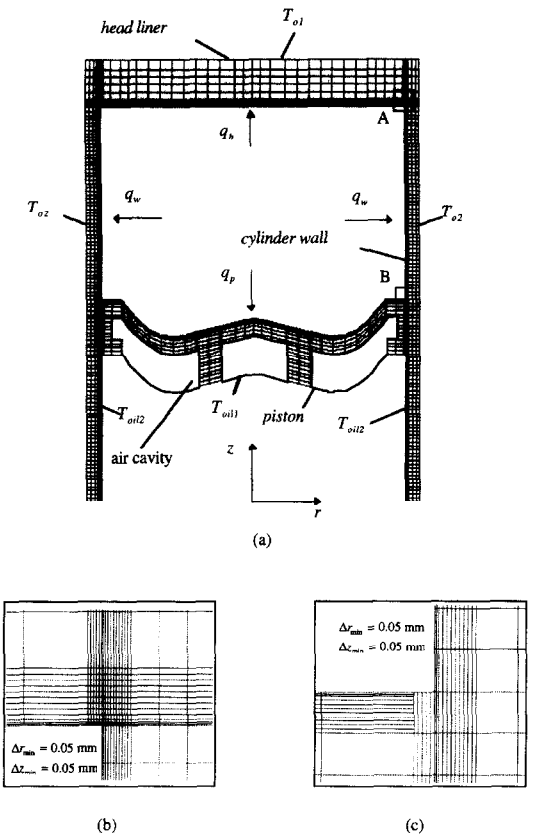

Fig. 7. Numerical mesh of Isuzu ceramic diesel engine at 90° ATDC: (a) combustion chamber mesh; (b) enlarged A; (c) enlarged B.

and it is 126 for the fine option. The grid size in z-direction is 1 mm within the cylinder wall and 0.05, 0.1, 0.2 or 2 mm with increasing depth below the head surface.

The gasket between the head liner and cylinder is made of a metal compressed material and its thermal resistance was neglected in the model. Piston rings and the gas between them occupy the gap between the piston and the cylinder wall. In order to include the effects of piston rings on heat conduction, the gap grids from the bottom of the piston to the fifth mesh point were given piston ring properties. The fine grids in the A and B regions of Fig. 7(a) are enlarged and shown in Figs 7(b, c).

The instantaneous temperature at a point located on the head liner surface has been measured for both motored and fired engine operation cases [12]. Based on the instantaneous surface temperature, the heat flux at this point was calculated using the transient heat conduction equation. For the motored case, the calculation time step is 2.78×10^{-5} s (i.e. 0.25 crank angle degree); the engine speed is 1500 rpm; and the cylinder coolant temperature is the measured value of 310.8 K. For the fired case, the calculation time step is 2.76×10^{-5} s; the engine speed is 1510 rpm and the cylinder coolant temperature is 354.7 K. For the motored case, the temperature above the head liner was designated as $T_{01} = 412.5$ K; the temperature outside the cylinder wall as $T_{02} = 310.8$ K, i.e. the same as the coolant temperature; and the temperature on the bottom surface of the piston and on the inner surface of the cylinder wall below the piston was specified as $T_{oil1} = T_{oil2} = 375$ K. For the fired case, the corresponding temperatures are $T_{01} = 645$ K, $T_{02} = 364.7$ K, $T_{oil1} = 675$ K and $T_{oil2} = 375$ K, respectively.

Figures 8(a, b) show comparisons between the computed and measured temperature at the monitoring point for the motored and fired cases, respectively. Note that, in this case the HCC code was run for 500 engine cycles (starting from the uniform wall temperature initial condition of $T = 355$ K) until a pseudo-steady state was reached (i.e. for the warmed up engine). The computed temperature in the measurement position is in good agreement with the measured temperature for both the motored and fired cases. These results strongly verify that the present heat conduction in components code (HCC) developed in this study is suitable for modeling the temperature distribution of the combustion chamber surfaces in engines. Figures 9(a, b) display the transient temperature variation at different depths into the

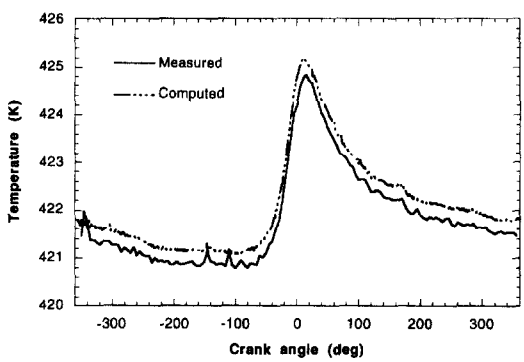

(a)

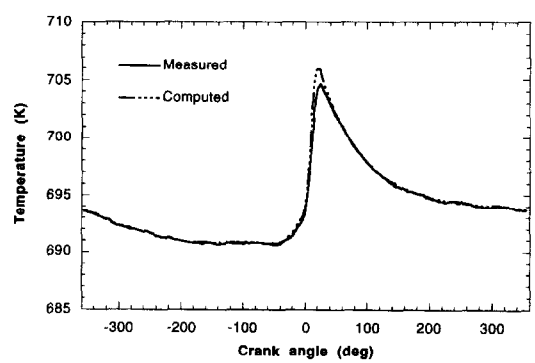

(b)

Fig. 8. Surface temperature comparison on the cylinder head for the Isuzu engine: (a) motored case; (b) fired engine case.

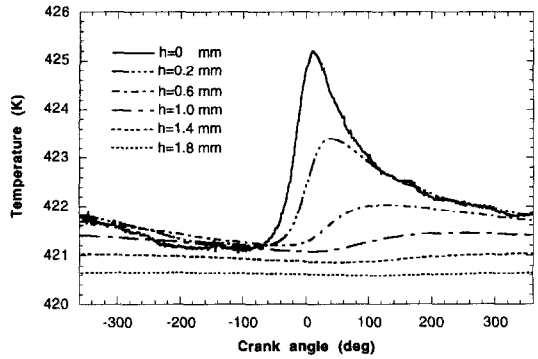

(a)

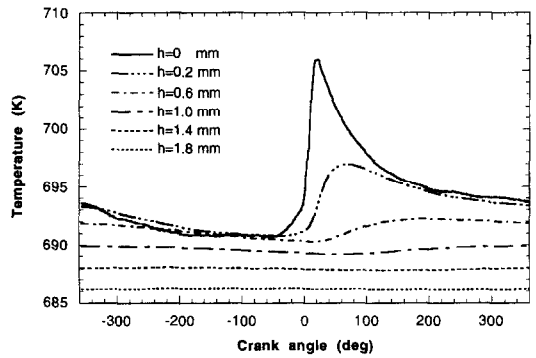

(b)

Fig. 9. Predicted temperature variation with depth into the head wall for the Isuzu engine: (a) motored case; (b) fired engine case.

metal below the head surface for the motored and fired cases, respectively. It can be concluded that when the depth exceeds about 1.0 mm, either for the motored or for the fired case, an obvious transient temperature variation can hardly be seen, which means the heat conduction below this depth obeys a kind of pseudo steady rule. This result agrees with the conclusions of Morel *et al.* [8].

As a final application example, the present HCC code was also applied to predict heat transfer in a Caterpillar diesel engine described in Table 2. It has a Mexican-hat bowl and a centrally-located high pressure fuel injector. The material of the cylinder wall, head and piston was assumed to be cast iron with density $\rho = 7870$ kg m^{-3}, thermal conductivity $k = 47.65$ W m^{-1} K^{-1} and specific heat $c_p = 447$ J kg^{-1} K^{-1}. The engine was cooled on the cylinder head and wall by the coolant water jacket and on the bottom of the piston by lubricating oil. The measured coolant temperature is 361 K and the measured oil temperature is 375 K [13]. The cylinder wall temperature below the piston is assumed to be an average value between the coolant and oil temperature, that is, 368 K.

A simplified finite difference model of the Caterpillar engine is shown in Fig. 10(a) for the fine grid option. The grid number density is 55 in the r-direction and 114 in the z-direction. The grid size is about 2 mm in each direction, except for the grids near the chamber surfaces, where the size is 0.05, 0.1, 0.5 or 1 mm depending on the depth below the surface. Regarding the temperature boundary conditions shown in Fig. 10(a), T_{01} and T_{02} were given as 361 K; $T_{oil1} = 375$ K and $T_{oil2} = 368$ K, according to the measured coolant and oil temperature [14]. When the calculations were

Table 2. Specifications of the Caterpillar diesel engine

Bore of cylinder	137.19	mm
Stroke	165.1	mm
Connecting rod length	261.62	mm
Displacement	2.44	L
Compression ratio	15.0	—
Piston crown	Mexican hat	—
Engine speed	1600	rpm
Intake pressure	182.7	kPa
Initial gas temperature	309	K
Injection timing	8.5	degrees BTDC
Intake-valve close timing	147	degrees BTDC

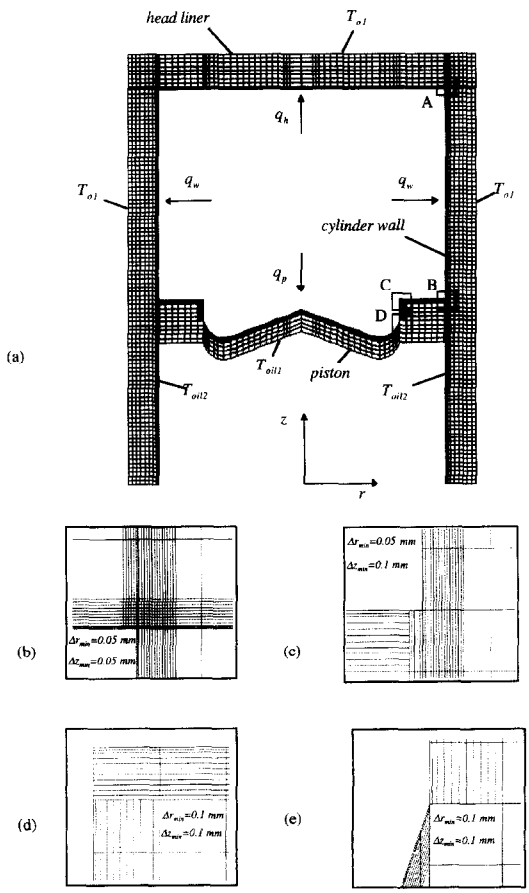

Fig. 10. Numerical mesh of the Caterpillar diesel engine at 90° ATDC: (a) combustion chamber mesh; (b) enlarged A; (c) enlarged B; (d) enlarged C; (e) enlarged D.

executed, the coarse grid option was computed for 900 engine cycles and then the fine grid option was used for an additional 50 engine cycles. This procedure was found to help ensure rapid convergence to pseudo steady-state [9]. The detailed fine grid arrangement is shown in Figs 10(b–e). The gasket between the cylinder head and wall is very thin in the Caterpillar engine, so its thermal resistance was neglected in the model. The calculation time step used was 1.04166×10^{-4} s and it corresponds to 1 degree of crank angle at 1600 rev min^{-1}.

An iteration scheme with the KIVA-II code [2] and the HCC code was also used in the calculations for the Caterpillar diesel engine. In the first iteration, the KIVA-II code was executed using assumed constant temperature wall surface boundary conditions; then the HCC code was run to obtain a first wall temperature distribution prediction, using the first heat flux data computed by KIVA-II as boundary conditions. In the second iteration, the KIVA-II code was executed again to compute improved heat flux boundary conditions, using the first temperature distributions from the HCC code as boundary conditions; then the HCC code was used to get the second temperature distributions, using the second heat flux data as boundary conditions. Finally, the KIVA-II code was used to calculate the third heat flux data, then the HCC code was used to obtain the final (converged) temperature distributions. More details of this iterative procedure and a discussion of the KIVA model used are given by Liu and Reitz [15] and Han and Reitz [3].

The computed time-averaged temperature distributions on each surface of the combustion chamber are shown in Fig. 11. For the cylinder head, the first temperature distributions, as shown in Fig. 11(a), are 50–120 K lower than the original (assumed) constant temperature, and have their maximum value at the edge of the bowl. The maximum time-averaged temperature difference at points on the surface is about 70 K. The second temperature distributions are a little higher than the first, but still lower than the original guess. The third temperature distributions are almost converged to the second, and the results show that the iterations have reached satisfactory results.

For the piston, the first temperature distributions, as shown in Fig. 11(b), are also lower than the original guess used in KIVA, and form a high temperature region on the bowl-side surface and a low temperature region on the bowl-valley surface. The second temperature distributions are seen to give a higher peak temperature than the first, especially on the bowl-side surface, where they are even higher than the original guess value. The average value of the second temperature distribution seems to be near the original, and this suggests that if a multidimensional combustion code must use constant temperature boundary conditions, the original (guessed) piston temperature may have been a reasonable value. The third temperature distributions also verify that the iterations

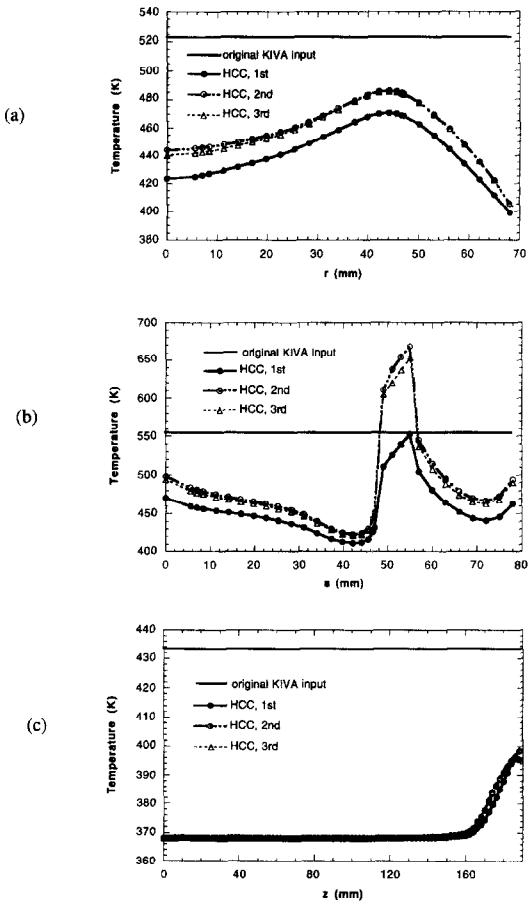

Fig. 11. Predicted time-averaged temperature distributions on the combustion chamber surfaces (a) cylinder head; (b) piston surface; (c) cylinder liner wall.

have converged. Figure 11(c) shows that the first, second and third temperature distributions on the cylinder wall surface are the same as the oil temperature adjacent to the wall for the majority of locations on the surface, but there is a 30 K increment in temperature in the region near the cylinder head. This shows that combustion and heat transfer within the cylinder do not have much influence on the temperature distribution of the wall surface, except for in a narrow region in the ring reversal region near the cylinder head.

The present HCC code provides an accurate and consistent method for obtaining the temperature distributions within engine components and these results would also be useful for structural analysis. In addition, combustion chamber wall temperatures have been shown to significantly influence engine NO_x emissions [15].

CONCLUSIONS

A two-dimensional (axisymmetric) transient heat conduction in components code (HCC) was suc-

cessfully developed in this study and extensively used to calculate the temperature field existing in realistic engine combustion chambers. The numerical method used in this study is the ADE Saul'yev finite difference method. This method is characterized by its explicit nature, unconditional numerical stability, and good accuracy, and is proved to be an effective tool for solving transient and pseudo-steady state heat conduction problems in engines.

Special treatments for the head gasket and the piston-liner air gap, and a grid transformation for describing the realistic piston bowl shape were designed and utilized in the present study. The methods were verified to be feasible for finite difference analysis through simplified test problem comparisons with the results of a finite element method (FEHT). The accomplishment of modeling piston movement within the present finite difference formulation makes the HCC code a computer program with the capability of realistic engine simulation.

The HCC code was used to calculate heat conduction processes occurring in the combustion chambers of an Isuzu ceramic engine and a Caterpillar diesel engine. For the Isuzu engine, the computed temperature swing at a point on the cylinder head is consistent with measured temperature data for both the motored and fired cases. This verifies that the HCC code is suitable for use to model temperature distributions on the combustion chamber surfaces of engines. The computed temperature swings at different depths into the metal below the cylinder head surface demonstrate that for a depth exceeding about 1.0 mm, the temperature profile exhibits pseudo-steady state characteristics. In addition, an iterative sequence that combines the KIVA code (for the gas-side heat transfer prediction) and the HCC code (for the wall temperature prediction) was developed. This combination is shown to provide more reasonable and accurate converged combustion chamber wall temperatures.

Acknowledgements—The authors thank Professor Gary Borman for his helpful comments. Stefan Simescu also deserves an acknowledgement for his generous help with valuable suggestions and useful experiment data. Cray Research, Inc., DOE/NASA-Lewis, Army Research Office and Caterpillar are acknowledged for their funding of this work.

REFERENCES

1. Borman, G. L. and Nishiwaki, K., Internal combustion engine heat transfer. *Progress in Energy Combustion Science*, 1987, **13**, 1–46.
2. Amsden, A. A., O'Rourke, P. J. and Butler, T. D., *KIVA-II: A Computer Program for Chemically Reactive Flows with Sprays*. Los Alamos National Labs, LA-11560-MS, 1989.
3. Han, Z. and Reitz, R. D., A temperature wall function formulation for variable-density turbulent flow with application to engine convective heat transfer modeling. *International Journal of Heat and Mass Transfer*, 1997, **40**(3), 613–625.
4. Saul'yev, V. K., *Integration of Equations of Parabolic Type by the Method of Nets*. Pergamon, New York, 1964, pp. 29–43.
5. Roache, P. J., *Computational Fluid Dynamics*. Hermosa, Albuquerque, NM, 1976.
6. Myers, G. E., *Analytical Methods in Conduction Heat Transfer*. McGraw-Hill, New York, 1971.
7. Heywood, J. B., *Internal Combustion Engine Fundamentals*. McGraw-Hill, New York, 1989.
8. Morel, T., Keribar, R. and Blumberg, P. N., Cyclical thermal phenomena in engine combustion chamber surfaces. SAE Technical Paper 850360, 1985.
9. Liu, Y., Modeling of combustion chamber surface temperatures with application to multidimensional diesel engine simulation. M.S. thesis, University of Wisconsin–Madison, 1996.
10. Klein, S. A., Beckman, W. A. and Myers, G. E., *FEHT: A Finite Element Analysis Program*. F-Chart Software, Madison, 1994.
11. Carslaw, H. S. and Jaeger, J. C., *Conduction of Heat in Solids*. Clarendon Press, Oxford, 1959, pp. 112–114.
12. Simescu, S., Heat flux measurements of the combustion chamber head surface of a silicon nitride D.I. diesel engine. Ph.D. thesis, University of Wisconsin–Madison, 1997.
13. Nehmer, D. A. and Reitz, R. D., Measurement of the effect of injection rate and split injections on diesel engine soot and NO_x emissions. SAE Technical Paper 940668, 1994.
14. Montgomery, D., An investigation of the effects of injection and EGR parameters on the emissions and performance of heavy duty direct injection diesel engines. M.S. thesis, University Wisconsin–Madison, 1997.
15. Liu, Y. and Reitz, R. D., Multidimensional modeling of engine combustion chamber surface temperatures. SAE Technical Paper 971593, 1997.

APPENDIX A

Transformed finite difference equations for non-uniform grids

The Saul'yev finite difference equations that correspond to eqn (1) can be transformed using the transformation eqns (8) and (9) as follows:

Let

$$h_1 = \xi_i - \xi_{i-1} = \Delta\xi_{i-1}; \quad h_2 = \xi_{i+1} - \xi_i = \Delta\xi_i;$$
$$h = h_1 + h_2 = \Delta\xi_{i-1} + \Delta\xi_i; \quad l_1 = \eta_j - \eta_{j-1} = \Delta\eta_{j-1};$$
$$l_2 = \eta_{j+1} - \eta_j = \Delta\eta_j; \quad l = l_1 + l_2 = \Delta\eta_{j-1} + \Delta\eta_j;$$
$$d_1 = z_i - z_{i-1} = \Delta z_{i-1}; \quad d_2 = z_{i+1} - z_i = \Delta z_i;$$
$$d = d_1 + d_2 = \Delta z_{i-1} + \Delta z_i = z_{i+1} - z_{i-1}.$$

Then the finite difference expression for the temperature in the left to right sweep is [9]

$$U_{i,j}^{k+1} = \left\{ \left(\frac{1}{2\alpha\Delta t} \right) U_{i,j}^{k} + \frac{1}{h_1 h_2 h} \left[h_1 \left(1 + \frac{h_2}{2\xi_i} \right) \times \left(U_{i+1,j}^{k} - U_{i,j}^{k} - \frac{d_2}{l} (U_{i,j+1}^{k} - U_{i,j-1}^{k}) \right) + h_2 \left(1 - \frac{h_1}{2\xi_i} \right) \left(U_{i-1,j}^{k+1} + \frac{d_1}{l} (U_{i,j+1}^{k} - U_{i,j-1}^{k}) \right) \right] + \frac{1}{l_1 l_2 l} \left(1 + \left(\frac{d}{h} \right)^2 \right) (l_1 (U_{i,j+1}^{k} - U_{i,j}^{k}) + l_2 U_{i,j-1}^{k+1}) \right\} \Bigg/ \left[\frac{1}{2\alpha\Delta t} + \frac{1}{h_1 h} \left(1 - \frac{h_1}{2\xi_i} \right) + \frac{1}{l_1 l} \left(1 + \left(\frac{d}{h} \right)^2 \right) \right] \tag{A1}$$

where $U_{i,j}^k = T_{i,j}^k$. With exactly the same procedure, the right to left sweep is

$$V_{i,j}^{k+1} = \left\{\left(\frac{1}{2\alpha\Delta t}\right)V_{i,j}^k + \frac{1}{h_1 h_2 h}\left[h_1\left(1+\frac{h_2}{2\xi_i}\right)\times\left(V_{i+1,j}^{k+1} - \frac{d_2}{l}(V_{i,j+1}^k - V_{i,j-1}^k)\right) - h_2\left(1-\frac{h_1}{2\xi_i}\right)\times\left(V_{i,j}^k - V_{i-1,j}^k + \frac{d_1}{l}(V_{i,j+1}^k - V_{i,j-1}^k)\right)\right] + \frac{1}{l_1 l_2 l}\left(1+\left(\frac{d}{h}\right)^2\right)\times(l_1 V_{i,j+1}^{k+1} - l_2(V_{i,j}^k - V_{i,j-1}^k))\right\}\Bigg/$$

$$\left[\frac{1}{2\alpha\Delta t} + \frac{1}{h_2 h}\left(1+\frac{h_2}{2\xi_i}\right) + \frac{1}{l_2 l}\left(1+\left(\frac{d}{h}\right)^2\right)\right] \quad \text{(A2)}$$

where $V_{i,j}^k = T_{i,j}^k$, and, finally

$$T_{i,j}^{k+1} = \tfrac{1}{2}(U_{i,j}^{k+1} + V_{i,j}^{k+1}) \quad \text{(A3)}$$

APPENDIX B

Boundary conditions in the transformed coordinate system

It is necessary to transform the boundary conditions from the physical to the computational domains (see Fig. 3). Assume that there exists an arbitrary function f in the cylindrical coordinate system, then its gradient can be expressed as

$$\nabla f = \frac{\partial f}{\partial r}\mathbf{i} + \frac{\partial f}{\partial z}\mathbf{j} = \left(\xi_r\frac{\partial f}{\partial \xi} + \eta_r\frac{\partial f}{\partial \eta}\right)\mathbf{i} + \left(\xi_z\frac{\partial f}{\partial \xi} + \eta_z\frac{\partial f}{\partial \eta}\right)\mathbf{j}.$$

The unit vector which is perpendicular to $f(r,z) = \text{const}$ and points in its increasing direction may be expressed as $\mathbf{n}^{(f)} = \nabla f/|\nabla f|$. Let $f = \xi$, then from eqn (B1), $\nabla\xi = \xi_r\mathbf{i} + \xi_z\mathbf{j}$ and $|\nabla\xi| = \sqrt{\xi_r^2 + \xi_z^2} = \sqrt{a}$, hence $\mathbf{n}^{(\xi)} = \nabla\xi/|\nabla\xi| = 1/\sqrt{a}(\xi_r\mathbf{i} + \xi_z\mathbf{j})$. In the same way $\mathbf{n}^{(\eta)} = 1/\sqrt{b}(\eta_r\mathbf{i} + \eta_z\mathbf{j})$, where $\sqrt{b} = \sqrt{\eta_r^2 + \eta_z^2}$. For the temperature on the boundary, its directional derivative is

$$\frac{\partial T}{\partial n^{(\xi)}} = \frac{\partial T}{\partial r}\cos(n^{\xi}, r) + \frac{\partial T}{\partial z}\cos(n^{(\xi)}, z)$$

where $\cos(n^{\xi}, r) = \mathbf{n}^{(\xi)}\cdot\nabla r = \xi_r/\sqrt{a}$ and $\cos(n^{(\xi)}, z) = \mathbf{n}^{(\xi)}\cdot\nabla z = \xi_z/\sqrt{a}$. Thus

$$\frac{\partial T}{\partial n^{(\xi)}} = \left(\xi_r\frac{\partial T}{\partial \xi} + \eta_r\frac{\partial T}{\partial \eta}\right)\frac{\xi_r}{\sqrt{a}} + \left(\xi_z\frac{\partial T}{\partial \xi} + \eta_z\frac{\partial T}{\partial \eta}\right)\frac{\xi_z}{\sqrt{a}}$$

$$= \frac{1}{\sqrt{a}}\left[(\xi_r^2 + \xi_z^2)\frac{\partial T}{\partial \xi} + (\xi_r\eta_r + \xi_z\eta_z)\frac{\partial T}{\partial \eta}\right]$$

$$= \frac{1}{\sqrt{a}}\left[a\frac{\partial T}{\partial \xi} + c\frac{\partial T}{\partial \eta}\right]$$

where $c = \xi_r\eta_r + \xi_z\eta_z$. Similarly

$$\frac{\partial T}{\partial n^{(\eta)}} = \frac{1}{\sqrt{b}}\left(c\frac{\partial T}{\partial \xi} + b\frac{\partial T}{\partial \eta}\right).$$

From the transformation equations (8) and (9), $\xi_r = 1$, $\xi_z = 0$, $\eta_r = -z_{i+1} - z_i/r_{i+1} - r_i$, $\eta_z = 1$.

Hence

$$a = 1, \quad b = 1 + \left(\frac{z_{i+1} - z_i}{r_{i+1} - r_i}\right)^2, \quad c = -\frac{z_{i+1} - z_i}{r_{i+1} - r_i}.$$

For the boundary nodes located on the cylinder center line, there are two kinds of nodal configurations, as shown in Figs 3(a, b), and their finite difference expressions may be written as follows, respectively:

$$U_{i,j} = [(c_{a1} + c_{a3})U_{i+1,j} + (c_{a2} + c_{a4})U_{i,j-1} + q_1''(1)]/(c_{a1} + c_{a2} + c_{a3} + c_{a4})$$

where

$$c_{a1} = -\frac{ck}{\sqrt{b}h_2}, \quad c_{a2} = \frac{\sqrt{b}k}{l_1}, \quad c_{a3} = \frac{2l_1 k}{h_2^2}$$

and $$c_{a4} = -\frac{2ck}{h_2},$$

and

$$U_{i,j} = [(c_{c1} + c_{c3} + c_{c5} + c_{c7})U_{i+1,j} + (c_{c2} + c_{c4})U_{i,j-1} + (c_{c6} + c_{c8})U_{i,j+1}]/(c_{c1} + c_{c2} + c_{c3} + c_{c4} + c_{c5} + c_{c6} + c_{c7} + c_{c8})$$

where

$$c_{c1} = -\frac{ck}{\sqrt{b}h_2}, \quad c_{c2} = \frac{\sqrt{b}k}{l_1}, \quad c_{c3} = \frac{2l_1 k}{h_2^2}, \quad c_{c4} = -\frac{2ck}{h_2}$$

$$c_{c5} = \frac{2l_2 k}{h_2^2}, \quad c_{c6} = \frac{2ck}{h_2}, \quad c_{c7} = \frac{ck}{\sqrt{b}h_2} \quad \text{and} \quad c_{c8} = -\frac{\sqrt{b}k}{l_2}.$$

For the nodal configuration shown in Fig. 3(c)

$$U_{i,j} = \left[(c_{d1} + c_{d3})U_{i-1,j} + (c_{d5} + c_{d7})U_{i+1,j} + (c_{d2} + c_{d4} + c_{d6} + c_{d8})U_{i,j-1} + \frac{c_{d9}}{2}(q_1''(i-1) + q_1''(i))\right]\Bigg/(c_{d1} + c_{d2} + c_{d3} + c_{d4} + c_{d5} + c_{d6} + c_{d7} + c_{d8})$$

where

$$c_{d1} = \frac{l_1 k}{h_1}\left(\xi_i - \frac{h_1}{2}\right), \quad c_{d2} = ck\left(\xi_i - \frac{h_1}{2}\right), \quad c_{d3} = \frac{ck}{\sqrt{b}}\left(\xi_i - \frac{h_1}{4}\right),$$

$$c_{d4} = -\frac{\sqrt{b}h_1 k}{l_1}\left(\xi_i - \frac{h_1}{4}\right) \quad c_{d5} = -\frac{ck}{\sqrt{b}}\left(\xi_i + \frac{h_2}{4}\right),$$

$$c_{d6} = \frac{\sqrt{b}h_2 k}{l_1}\left(\xi_i + \frac{h_2}{4}\right), \quad c_{d7} = \frac{l_1 k}{h_2}\left(\xi_i + \frac{h_2}{2}\right),$$

$$c_{d8} = -ck\left(\xi_i + \frac{h_2}{2}\right)$$

and

$$c_{d9} = h_1\left(\xi_i - \frac{h_1}{4}\right) + h_2\left(\xi_i + \frac{h_2}{4}\right).$$